Invited paper

OPTO-ELECTRONICS REVIEW 7(4), 253–258 (1999)

Uncooled IR focal plane arrays

P.W. KRUSE

Consultant, Infrared Technology, 6828 Oaklawn Ave., Edina, MN 55435, USA

Uncooled IR focal plane arrays employ thermal detection mechanisms including the resistive bolometric, pyroelectric, and thermoelectric effects. Readout electronics are incorporated at each pixel. Two thermal isolation structures are possible: hybrid and monolithic. The ultimate limit to the performance is set by temperature fluctuation noise, which depends upon the structure. The state-of-the-art of the approaches employing the three mechanisms is reviewed.

Keywords: uncooled IR focal plane arrays, bolometers, pyroelectric detectors, thermoelectric detectors.

1. Introduction

Uncooled infrared focal plane arrays are linear or two-dimensional assemblies of picture elements (pixels) which respond to infrared radiation without requiring cryogenic operation. The focal plane arrays of most interest are employed in thermal imaging of ambient temperature objects. For most applications, this requires that the arrays must respond to radiation in the 3–5 μm or 8–12 μm atmospheric windows.

Infrared detection mechanisms fall into three broad classes: photon, thermal and wave interaction. In the evolution of modern thermal imaging systems, it was the photon detectors which played the major role. The earliest systems employed two-dimensional scanning mechanisms. Thus a single detector scanned the entire image in one frame time, which in the U.S. was usually 1/30 s. Thus very fast detector response, typically in the microsecond range, was required. Photon detectors alone offered both broad spectral bandwidth and fast response. (Hg,Cd)Te was the preferred material, operating at 77 K. Later approaches employed linear arrays with a one-dimensional scan in 1/30 second, such as employed in the U.S. common modular FLIR. Although the speed of response requirement was thereby reduced, nevertheless only photon detectors such as (Hg,Cd)Te could meet both the sensitivity and speed of response requirement for applications requiring 1/30 s frame time. Thus, cryogenic operation was still required.

With the advent of two-dimensional arrays, howver, the frame time and the pixel response time became the same, i.e., 1/30 s for most U.S. systems. Thus, it became possible to consider approaches other than those employing photon detectors such as (Hg,Cd)Te, InSb, PbSe, AlGaAs/GaAs and PtSi, all of which require cryogenic operation. It is relatively straightforward to design a pixel employing a thermal detection mechanism which combines high sensitivity with 1/30 s response time but it is extremely difficult to design one with high sensitivity and a response time in, say, the microsecond range. Thus it was the advent of two-dimensional focal plane array technology which brought about the employment of thermal detection mechanisms.

2. Thermal detection mechanisms

Thermal detection mechanisms are those which depend upon the change in some property of a material due to a change in temperature of the material which accompanies the absorption of electromagnetic radiation. They do not depend upon the photon nature of the radiation. As a result, there is no long wavelength limit associated with an energy gap or donor/acceptor ionization energy such as is true for photon detectors. It is the optical absorption properties of the thermal detection mechanism and the pixel structure which determines the spectral response.

Many thermal detection mechanisms exist. When they are considered in light of the requirement for in-

tegration in large arrays, three emerge as the principal candidates: resistive bolometers, pyroelectric detectors and thermoelectric detectors. Each is discussed below.

2.1. Resistive bolometers [1]

The operation of a resistive bolometer is based upon the change in electrical resistance of a material which is caused by a change in temperature of that material due to absorbed radiant energy. The responsivity R of a resistive bolometer sensitive element is given by

$$R = \frac{I_b \alpha R_e \eta}{G(1+\omega^2\tau^2)^{1/2}}, \tag{1}$$

where I_b is the electrical bias current, R_e is the electrical resistance of the sensitive element, η is the absorptance of the material, G is the thermal conductance between the sensitive element and its support structure, ω is the angular modulation frequency of the incident radiation, α is the temperature coefficient of resistance and τ is the thermal response time. Here α and τ are given by

$$\alpha = \frac{1}{R_e}\frac{dR_e}{dT}, \tag{2}$$

and

$$\tau = \frac{C}{G}, \tag{3}$$

where C is the heat capacity of the sensitive element. The value of α is positive for metals and negative for semiconductors at room temperature. Typical values of α at room temperature are

metals: 0.002 K^{-1};
semiconductors: –0.02 K^{-1}.

2.2. Pyroelectric detectors [2]

The pyroelectric effect is found in certain ferroelectric crystals which exhibit spontaneous electric polarization, measured as a voltage between electrodes attached to the sample. In contrast to resistive bolometers and thermoelectric detectors, pyroelectric detectors show no dc response. If modulated radiation is absorbed by the crystal, a photocurrent is developed which is proportional to the time rate of change of temperature, given by

$$I_s = pA_D\frac{dT}{dt}, \tag{4}$$

where I_s is the photocurrent, p is the pyroelectric coefficient, which is a function of the chosen material, A_D is the crystal area and dT/dt is the rate of change of the crystal temperature T with time t.

The responsivity R of a pyroelectric detector is given by

$$R = \frac{\eta\omega pA_D r}{G(1+\omega^2\tau_e^2)^{1/2}(1+\omega^2\tau^2)^{1/2}}, \tag{5}$$

where r is the parallel resistance of the sensitive element and the readout electronics input, τ_e is the electrical time constant and the other symbols have been previously defined. The values of r and τ_e are given by

$$r = \frac{1}{\omega C_e \tan\delta}, \tag{6}$$

and

$$\tau_e = rC_e. \tag{7}$$

Here $\tan\delta$ is the loss tangent of the pyroelectric material and C_e is the pixel capacitance.

2.3. Thermoelectric detectors [3]

A thermoelectric detector, also known as a radiation thermocouple, includes two junctions between two differing electrical conductors. One junction is exposed to the incident radiation and is thereby heated; the other (shielded) junction is not. If one conductor is cut open, a voltage difference will be found between the exposed ends. The responsivity R of a thermoelectric detector is

$$R = \frac{NS\eta}{G(1+\omega^2\tau^2)^{1/2}}, \tag{8}$$

where S is the Seebeck coefficient of the junction between the materials. By series connecting pairs of exposed and shielded detectors, the voltage can be increased; this is known as a radiation thermopile. The responsivity is proportional to N, the number of thermocouples in electrical series.

Note that the responsivity of the radiation thermocouple is inversely proportional to the thermal conductance G, as is also true for that of the resistive bolometer and the pyroelectric detector.

3. Fundamental performance limits

The fundamental limit to the performance of any infrared detector based upon thermal detection principles is set by temperature fluctuation noise [4]. The value of D^*_{TF}, the temperature fluctuation noise limited D^*, is

$$D^*_{TF} = \left(\frac{\eta^2 A_D}{4kT_D^2 G} \right)^{1/2}, \tag{9}$$

where A_D is the detector area, equal to the pixel area in an array, k is the Boltzmann's constant, and T_D is the detector temperature. If the dominant method of exchanging heat between the pixel and its surroundings is radiative, then the temperature fluctuation noise limit converts to the background fluctuation noise limit, given by [4]

$$D^*_{TF} = \left[\frac{\eta}{8k\sigma(T_D^5 + T_B^5)} \right]^{1/2}, \tag{10}$$

where σ is the Stefan-Boltzmann constant and T_B is the background temperature.

The expression for the noise equivalent temperature difference, NETD, of an imaging array is

$$NETD = \frac{(4F^2 + 1)V_N}{A_D \tau_0 R (\Delta P/\Delta T_s)_{\lambda_1 - \lambda_2}}, \tag{11}$$

where F is the f/# of the optics, V_N is the electrical noise within the system bandwidth, τ_0 is the transmittance of the optics and $(\Delta P/\Delta T_s)_{\lambda_1 - \lambda_2}$ is the rate of change with temperature of the radiated power per unit area of a blackbody of temperature T_s, measured within the spectral interval from $\lambda_1 - \lambda_2$. The value of $(\Delta P/\Delta T_s)_{\lambda_1 - \lambda_2}$ for T_s of 300 K and $\lambda_1 - \lambda_2$ between 8 μm and 14 μm is 2.62×10^{-4} W/cm^{2}K.

Combining Eqs. (9) and (11) gives rise to the expression for $NETD_{TF}$, the NETD of a temperature fluctuation noise limited detector

$$NETD_{TF} = \frac{2(4F^2 + 1)T_D (kGB)^{1/2}}{\eta A_D \tau_0 (\Delta P/\Delta T_s)_{\lambda_1 - \lambda_2}}, \tag{12}$$

where the defining relationship between D^* and R

$$D^* = \frac{(A_D B)^{1/2} R}{V_N}, \tag{13}$$

has been employed. Here B is the electrical bandwidth.

Similarly, combining Eqs. (10) and (11) and (13) gives rise to the background fluctuation noise limited NETD, i.e., $NETD_{BF}$

$$NETD_{BF} = \frac{(4F^2 + 1)}{\tau_0 (\Delta P/\Delta T_s)_{\lambda_1 - \lambda_2}} \left[\frac{8kT\sigma B(T_D^5 + T_B^5)}{\eta A_D} \right]^{1/2}, \tag{14}$$

Figure 1 illustrates Eqs. (12) and (14) for the parameters assumed in the figure. All thermal infrared detectors fall on or above the limits shown. A detector structure with a given value of G cannot have an NETD better than (i.e., lower than) that point on the sloping line. Real detectors usually lie above the corresponding point because of noise greater than temperature fluctuation noise. No detector having the parameters shown can have an NETD better than (i.e., lower than) the background limit shown.

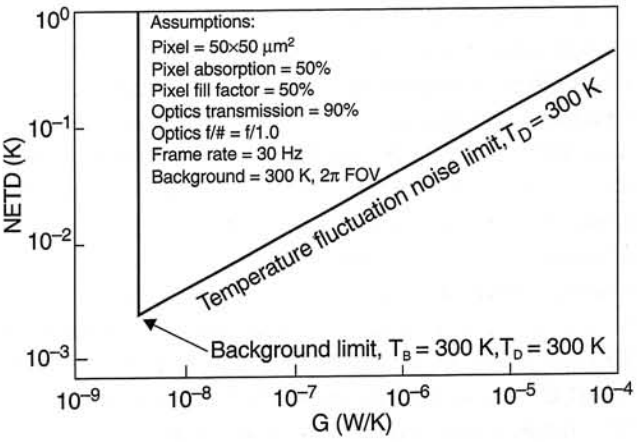

Fig. 1. Temperature fluctuation noise limit and background fluctuation noise limit of uncooled thermal imaging arrays employing thermal detection mechanisms.

4. State-of-the-art

The state-of-the-art of each of the principal detection mechanisms as of ca. 1995 can be found in Kruse and Skatrud. [5] The discussion below summarizes the early work and includes advances reported as late as 1999.

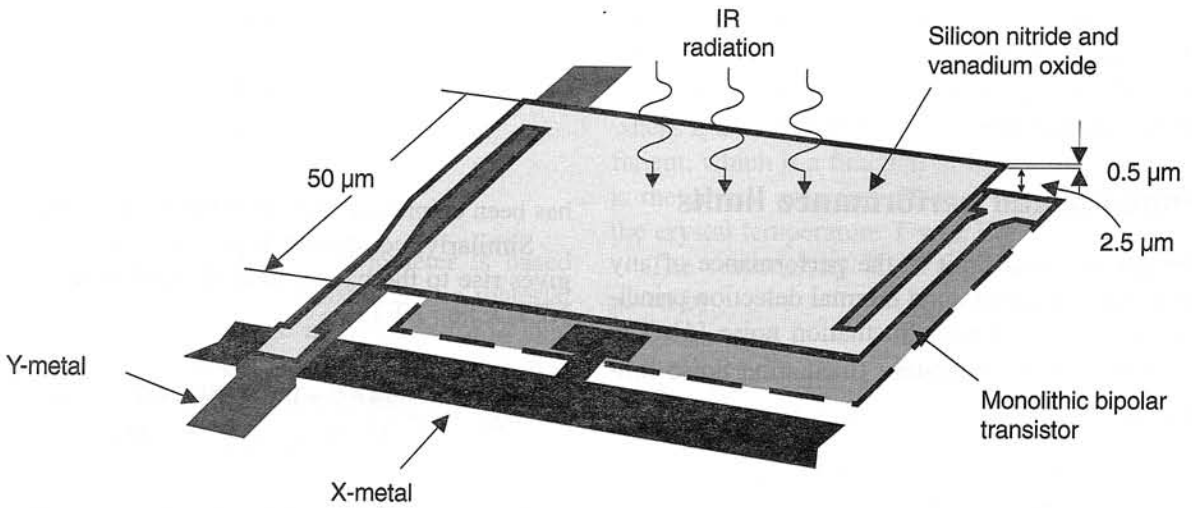

Fig. 2. Microbolometer pixel structure (after Ref. 7).

4.1. Resistive bolometer array

In 1992 and 1993, Wood and his colleagues [6,7], at Honeywell described the construction and performance of an 80,640 pixel uncooled bolometer array operating in the 8–12 μm spectral interval. Organized into 240 rows and 336 columns with 50×50 μm pixels, it operated at 30 Hz frame rate. The arrays employed silicon microstructure technology in which a silicon nitride membrane formed the thermal isolation structure, see Fig. 2. The pixel thermal conductance was 8×10^{-8} W/K, whereas the pixel heat capacity was 8×10^{-10} J/K. A film of vanadium oxide deposited upon the silicon nitride was the bolometric film; its thickness was much less than 1 μm. Each pixel included a transistor embedded in the silicon substrate to act as a self-closing switch. When operated at 30 frames per second with f/1 optics, the NETD was 0.040°C. There was no measurable optical crosstalk. No chopper was required. The thermal imagery was superior to that of cryogenic one-dimensional scanned (Hg,Cd)Te arrays and approached that of cryogenic two-dimensional (Hg,Cd)Te arrays.

Rather than continuing the development and entering into production of arrays, Honeywell chose to license them to three U.S. companies, Raytheon, Boeing and Lockheed-Martin. Each redesigned the read-out integrated circuit (ROIC) which underlay the silicon microstructure vanadium oxide bolometer array so as to improve the overall performance. At first they made little or no modifications of the vanadium oxide bolometric array; that is now changing. Recent developments are summarized below.

Radford and colleagues [8] at Raytheon have reported a 240×320 pixel array with 50 μm square vanadium oxide pixels, for which the average pixel NETD (f/1 optics) was 8.6 mK. However, the pixel response time was 29 ms, which is greater than optimum for 30 Hz frame rate. They also reported a 240×320 pixel array with 25 μm square vanadium oxide pixels with an average NETD (f/1 optics) of 52 mK.

Altman and colleagues [9] at Lockheed-Martin have reported development of a 640×480 pixel array with 28 μm square pixels with an average NETD (f/1 optics) of about 60 mK. However, this measurement was made on a "small pixel test lot," not on a full array.

Efforts are underway at Infrared Solutions, Inc. [10] and a joint program at Indigo and Boeing [11] to reduce the cost, size and power of uncooled bolometric thermal imagers by reducing the number of pixels to 160×120 (Infrared Solutions, Inc.) or 160×128 (Indigo/Boeing), while maintaining the pixel size at 50 μm square. The impact of reducing the number of pixels is found not only in reducing the array processing cost (more arrays per wafer, greater array yield) but also in simplifying, and thereby reducing the cost of the off-chip electronics.

Investigations are also underway to attempt to increase array performance by replacing vanadium oxide with a material having a higher temperature coefficient of resistance. The most promising material appears to be amorphous silicon under development at Raytheon by Brady and colleagues [12], but it is too early to tell whether it or any other material will replace vanadium oxide in the near term.

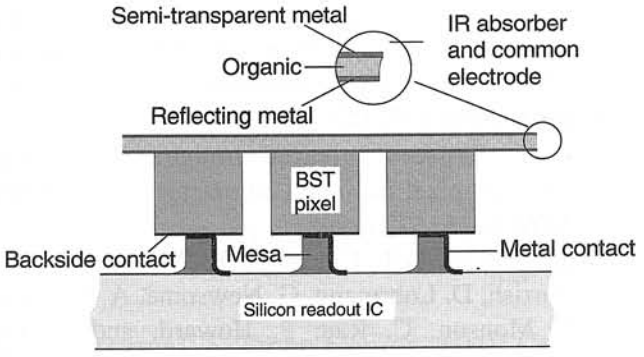

Fig. 3. Pyroelectric detector device structure (after Ref. 13).

4.2. Pyroelectric array

Hanson and his colleagues [13,14] at Texas Instruments (now Raytheon) have described the construction and performance of an uncooled pyroelectric array in which an electrical bias is employed to improve the performance. It is referred to as a field-enhanced pyroelectric array or a ferroelectric bolometer array. This is a hybrid structure in which infrared detection occurs in the ferroelectric material barium strontium titanate (BST) and bandpass amplification occurs in a silicon multiplexer bump-bonded at each pixel, see Fig. 3. The pixel thermal conductance is 2×10^{-6} W/K. With 245×328 pixels, each 50×50 μm, the measured NETD with f/1 optics at 30 frames per second is 0.05°C. A very small amount of optical crosstalk is detectable in the image. The array employs a radiation chopper.

Although many applications for this hybrid array technology have been identified, and imagers employing these arrays are in mass production, no hybrid technology advances are foreseen. The reason is that the thermal conductance of the bump bonds is so high that the array NETD (f/1 optics) is limited to about 50 mK.

Pyroelectric array technology therefore is moving toward monolithic silicon microstructure technology at Raytheon, as reported by Belcher and colleagues [15]. Furthermore, barium strontium titanate, which is not a good pyroelectric material in thin film form, is being replaced by lead titanate. Because the temperature at which ferroelectric materials such as barium strontium titanate and lead titanate lose their ferroelectric properties, known as the "Curie point" is far above room temperature for lead titanate, it turns out that uncooled lead titanate operates in only the pyroelectric mode. This possible disadvantage turns out to be an advantage, in that a temperature stabilizer is not required. Furthermore, electrical bias is not required, so that there is no excess, 1/f power law, noise.

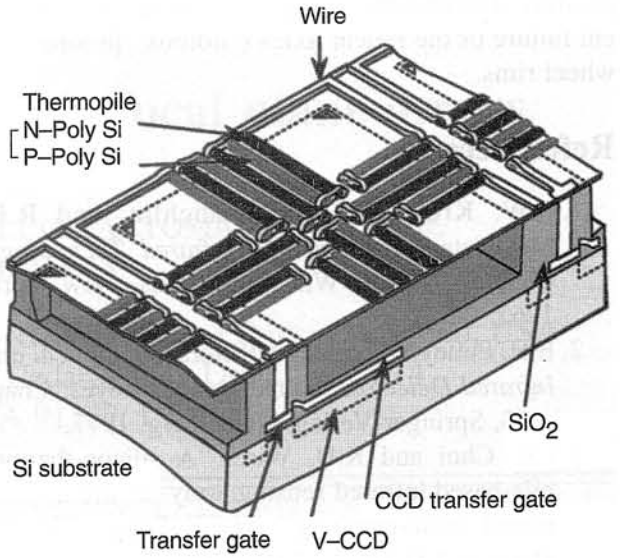

Fig. 4. Pixel structure for thermopile infrared focal plane array (after Ref. 16).

4.3. Thermoelectric array

Kanno [16] and his colleagues have described the construction and performance of an uncooled monolithic silicon array incorporating 128×128 pixels, each 100×100 μm. Detection occurs in a 32 element thermopile, consisting of p-type and n-type polysilicon thermocouples, deposited upon a silicon dioxide membrane at each pixel, see Fig. 4. The frame rate is 120 Hz. The NETD is 0.5°C with an f/1 lens. No chopper is required.

McManus and Mickelson [17] of Infrared Solutions, Inc., have described a family of imaging radiometers which employ silicon microstructure linear thermoelectric arrays using chromel-constantan thin film thermocouples. One example employs a 120 pixel linear array which is mechanically scanned across the focal plane of an f/0.7 germanium lens in 1.44 s. The NETD is 0.35°C. Because it is a radiometer, temperature measurement accuracy is an important parameter; the value is 2°C or 2% of full scale over the range from 0°C to 350°C. The primary application is in industrial predictive and preventive maintenance. Another example is a linescanner, which measures the temperature profiles of railcar wheels moving at railcar speeds of up to 80 miles per hour. Computation within the linescanner of the tem-

perature distribution is employed to identify incipient failure of the railcar axles ("hotbox" problem) or wheel rims.

References

1. P.W. Kruse, L.D. McGlauchlin, and R.B. McQuistan, *Elements of Infrared Technology*, Chapter 9, John Wiley and Sons, New York, 1962.
2. E.H. Putley, "Thermal detectors", in *Optical and Infrared Detectors*, edited by R.J. Keyes, Chapter 3, Springer-Verlag; Heidelberg, 1977.
3. I.H. Choi and K.D. Wise, "A silicon-thermopile-based infrared sensing array for use in automated manufacturing", *IEEE Trans. Electron Devices*. **ED-33**, 72–79 (1986).
4. P.W. Kruse, L.D. McGlauchlin, and R.B. McQuistan, op. cit. 1.
5. *Uncooled infrared imaging arrays and systems*, edited by P.W. Kruse and D.D. Skatrud, *Semiconductors and Semimetals*, Vol. 47, Academic Press, San Diego, 1997.
6. R.A. Wood, C.J. Han, and P.W. Kruse, "Integrated uncooled infrared imaging arrays", *IEEE Solid State Sensor and Actuator Workshop*, pp. 132-135, Hilton Head Island, S.C., 1992.
7. R.A. Wood, "Uncooled thermal imaging with monolithic silicon focal plane arrays", *Proc. SPIE* **2020**, 322–329 (1993).
8. W. Radford, D. Murphy, A. Finch, K. Hay, A. Kennedy, M. Ray, A. Sayed, J. Wyles, R. Wyles, J. Varesi, E. Moody, and F. Cheung, "Sensitivity improvements in uncooled microbolometer FPA's", *Proc. SPIE* **3698**, 119–130 (1999).
9. M. Altman, B. Backer, M. Kohin, R. Blackwell, N. Butler, and J. Cullen, "Lockheed Martin's 640×480 uncooled microbolometer camera", *Proc. SPIE* **3698**, 137–143 (1999).
10. P.W. Kruse, "Infrared imager employing 160×120 pixel uncooled bolometer array", *Proc. SPIE* **3436**, 572 (1998).
11. J.L. Heath, G.T. Kincaid, J.T. Woolaway, W.J. Parrish, D. Lohrmann, G. Newsome, A. Inosecu, J. Monson, C. Rau, P. Howard, and C. Li, "160×128 uncooled FPA performance review", *Proc. SPIE* **3698**, 256–263 (1999).
12. J. Brady, T. Schimert, D. Ratcliff, R. Gooch, B. Ritchey, P. McCardel, K. Rachels, S. Ropson, M. Wand, M. Weinstein, and J. Wynn, "Advances in amorphous silicon uncooled IR systems", *Proc. SPIE* **3698**, 161–167 (1999).
13. C.M. Hanson, H. Beratan, R. Owen, M. Corbin, and S. McKenney, "Uncooled thermal imaging at Texas Instruments", *Proc. SPIE* **1735**, 17–26 (1992).
14. C.M. Hanson, "Uncooled ferroelectric thermal imaging", *Proc. SPIE* **2020**, 330–339 (1993).
15. J.F. Belcher, "Uncooled monolithic ferroelectric IRFPA technology", *Proc. SPIE* **3436**, 611 (1998).
16. T. Kanno, M. Saga, S. Matsumoto, M. Uchida, N. Tsukamoto, A. Tanaka, S. Itoh, A. Nakazato, T. Endoh, S. Tohyarna, Y. Yamamoto, S. Murashima, M. Fujimoto, and N. Teranishi "Uncooled infrared focal plane array having 128×128 thermopile detector elements", *Proc. SPIE* **2269**, 450–459 (1994).
17. T. McManus and S. Mickelson, "Imaging radiometers employing linear thermoelectric arrays", *SPIE* **3698**, 352–360 (1999).

